Quaternary Research (2019), **91**, 35–50

doi:10.1017/qua.2018.64

THEMATIC SET
DRYLANDS

Aeolian influx and related environmental conditions on Gran Canaria during the early Pleistocene

Inmaculada Menéndez[a]*, José Mangas[a], Esperança Tauler[b], Vidal Barrón[c], José Torrent[c], Juan F. Betancort[d], Ángelo Santana[e], José Manuel Recio[f], Luis A. Quevedo-González[a], Ignacio Alonso[a], Jorge Méndez-Ramos[g]

[a]Instituto de Oceanografía y Cambio Global, IOCAG, Universidad de Las Palmas de Gran Canaria, Campus Tafira, 35017 Las Palmas de Gran Canaria, Spain
[b]Departamento de Mineralogia, Petrología y Geología Aplicada, Universitat de Barcelona, Martí i Franqués, 08028 Barcelona, Spain
[c]Departamento de Agronomía, Universidad de Córdoba, Campus de Rabanales, 14071 Córdoba, Spain
[d]Universidad Nacional de Educación a Distancia (UNED), Juan del Rosal, 14, 28040 Madrid, Spain
[e]Departamento de Matemáticas, Universidad de Las Palmas de Gran Canaria, Campus de Rabanales, 14071 Córdoba, Spain
[f]Departamento de Ecología (Geografía Física), Universidad de Córdoba, Campus de Rabanales, 14071 Córdoba, Spain
[g]Departamento de Física, Universidad de La Laguna, Campus San Cristobal de la Laguna, 38200 Tenerife, Spain

(Received September 14, 2017; Accepted May 25, 2018

Abstract

The island of Gran Canaria is regularly affected by dust falls due to its proximity to the Saharan desert. Climatic oscillations may affect the Saharan dust input to the island. Geochemical, mineralogical, and textural analysis was performed on a well-developed and representative early Pleistocene paleosol to examine Saharan dust contribution to Gran Canaria. Significant and variable Saharan dust content was identified in addition to weathering products such as iron oxides and clay minerals. Variations in quartz and iron oxide concentrations in the paleosol likely reflect different Saharan dust input in more/less-contrasted rhexistasic/biostatic climatic conditions. Linking the quartz content in Canarian soils, the Ingenio paleosol, and two Canarian loess-like deposits to different ages from the Quaternary, we hypothesized that the dust input should be lower (about 33–38%) throughout the early to middle Pleistocene than during the late Quaternary. The Saharan dust input to the Gran Canaria profile in the Pleistocene persisted in spite of climatic variations.

Keywords: Saharan dust; Dust deposits; Paleosols; Pleistocene; Canary Islands

INTRODUCTION

The Pleistocene Epoch is characterized by a cyclic growth and decline of continental ice-sheets that can be identified by benthic $\delta^{18}O$ records (Fig. 1; Lisiecki and Raymo, 2005). Regarding the starting point of this epoch, the International Union of Geological Sciences (IUGS) ratified the Gelasian Stage with an onset 2.58 Ma ago as the basal stage of the Pleistocene (Gibbard and Head, 2009). The base of the Gelasian is detectable in marine and continental records, and characterized by the appearance of loess sedimentation in China (Kukla and Han, 1989) and the decrease of tropical forest (Leroy, 2007). The most accepted worldwide proxy datum for the Plio-Pleistocene boundary, however, is based on reversals of the earth magnetic field (Cita and Pillans, 2010). During Marine Oxygen Isotope Stages (MIS) 100 and 98, around 2.5 Ma ago, the establishment of the Saharan desert and the onset of trade winds took place, setting important changes in the climate of northwest Africa. This was coincident with the stepwise intensification of the Northern Hemisphere ice sheet buildup (Dupont and Leroy, 1995). During these times as well as during all Gelasian-Calabrian stages, climatic cycles were primarily driven by obliquity-paced (41 ka) variability (Shackleton et al., 1995). Afterwards, the Gelasian-Calabrian stages with a relatively high frequency and short time span of glacial-interglacial cycles were replaced by the Ionian Stage with longer glacial and short interglacial periods (Cita and Pillans, 2010). Regarding the general climate conditions during the Gelasian–Calabrian stages, pollen spectra from the ocean core of Ocean Drilling Program site 658 (21°N, 19°W) indicate that glacial periods corresponded to strong aridity even in northwest Africa (Dupont and Leroy, 1995; Hooghiemstra et al., 2006).

Beside marine records, terrestrial archives likewise provide an important proxy for the Quaternary. In this sense, the

*Corresponding author at: Instituto de Oceanografía y Cambio Global, IOCAG, Universidad de Las Palmas de Gran Canaria, Campus Tafira, 35017 Las Palmas de Gran Canaria, Spain. E-mail address: inmaculada.menendez@ulpgc.es (I. Menéndez).

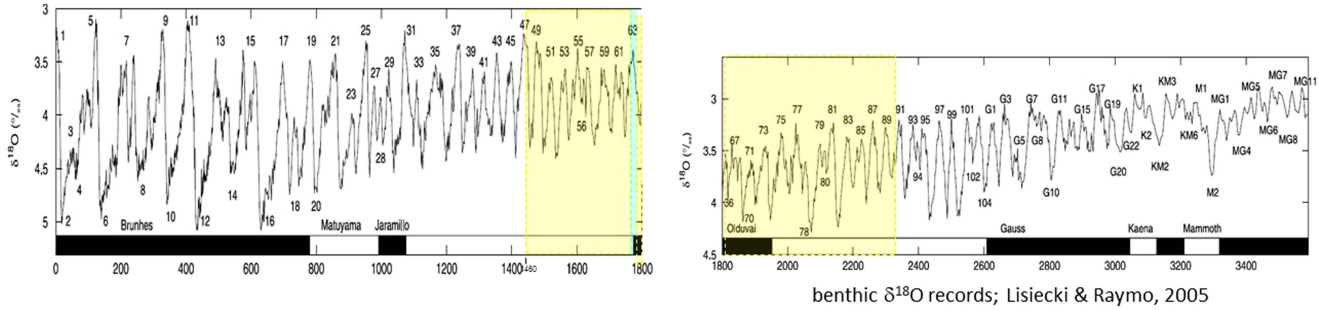

Figure 1. Benthic $\delta^{18}O$ records from the upper Pliocene to Holocene, compiled and published by Lisiecki and Raymo (2005). The yellow shaded square marks the Lower Pleistocene age of the Ingenio paleosol. In blue, Marine Oxygen Isotope (MIS) interglacial Stage 63 attributed to Agaete deposits. (For interpretation of the references to color in this figure legend, the reader is referred to the web version of this article.)

intensification of aeolian activity and the higher production of windblown deposits (e.g., continental dune fields and loess) are often regarded as indicators of serious aridity. This has been shown by numerous studies that associated aeolian deposits from continental environments with drier episodes during glacial, but also during interglacial, periods or even during the Holocene (Forman et al., 2001; Wolfe et al., 2004; Küster et al., 2006; Mason et al., 2007; Muhs et al., 2007; Wolfe and Hugenholtz, 2009; Lu et al., 2010; Yu and Lai, 2012; Qiang et al., 2013, 2016; Lehmkuhl et al., 2014; Zhang et al., 2015). When focusing on coastal environments, it has been shown that coastal dune fields expand as sea- and lake-water levels fall during glacial periods (Loope and Arbogast, 2000; Arbogast and Packman, 2004; Timmons et al., 2007; Hansen et al., 2010; Campbell et al., 2011). This relation also applies to the Canary Islands, however, where glacial periods are partly linked to more humid environmental conditions (Suchodoletz et al., 2009b; Roettig et al., 2018). This discrepancy illustrates that the accumulation of aeolian deposits might be strongly influenced by local or regional conditions such as the presence of unconsolidated sand- and silt-sized material/deposits, topography, wind speed, hydrology conditions, and vegetation status (Újvári et al., 2016; Liu et al., 2017).

Another consequence of aridity is the intensification of the aeolian flux into the sea (lithogenic flux). In the Eastern Mediterranean, as well as in the Canary Basin (Henderiks et al., 2002) and northwestern Africa, cold and dry conditions favored the dust flux (Hamann et al., 2008) and resulted in higher dust deposition during glacial times. On the other hand, higher lithogenic fluxes into the Mediterranean Basin have also been registered in relation to warm and dry conditions (Ehrmann et al., 2017). From this, it follows that dryness, rather than temperature, seems to be an enhancing factor of dust enrichment in marine deposits, which may be modified by local or regional conditions and the latitudinal range. Dust input likewise has a strong impact on terrestrial environments since aeolian sediments are one of the main components of arid soils (Offer et al., 1998; Neff et al., 2008) and other soils affected by dust plumes in areas adjacent to deserts. This is undoubtedly the case in the Canary Islands, located in close proximity to the Sahara (Criado and Dorta, 2003; Menéndez et al., 2007; 2009b; Suchodoletz et al., 2008, 2009a, 2009b, 2013), and even in the more distant Caribbean (Prospero and Lamb, 2003; Muhs et al., 1990, 2007).

When attempting to reconstruct climatic conditions based on the appearance and characteristics of soils, it is essential to consider the dust input that may have strongly influenced secondary mineral enrichment. A number of valuable proxies can be used to characterize pedogenesis and related environments. In particular, iron oxides are constantly present as secondary minerals in soils, and their typology and amount are good proxies for climate (Barrón and Torrent, 2013; Long et al., 2016; Zhao et al., 2017). Common iron oxide phases in well-aerated soils and sediments are hematite (Hm, α-Fe2O3), goethite (Gt, α-FeOOH), and maghemite (Mgh, γ-Fe2O3). The Hm / (Gt + Hm) ratio demonstrates a monotonic correlation with rainfall across a wide range of climate regimes (Schwertmann, 1985; Ji et al., 2001; Balsam et al., 2004; Zhang et al., 2009; Long et al., 2011, 1016). Moreover, iron and manganese minerals were found to influence the distribution of rare earth element (REE) distribution, due to the higher adsorptive affinity of light REE to soil minerals in comparison with heavy REE (Chang et al., 2016). REEs have been widely used to trace fundamental geochemical processes in soils, with a focus on weathering, the transformation and formation of REE-bearing minerals, adsorption, solubility and transport factors, and REE vertical distribution (Tyler, 2004; Sadeghi et al., 2013; Santana et al., 2015; Bern et al., 2017). All of these parameters, however, may also be modified by aeolian sediment input. Thus, a major concern is to evaluate the quantity of dust input to the soils and its impact on soil properties.

The aim of our study is to contribute to the understanding of aeolian input on soils and related climatic conditions during the early Pleistocene on the Canarian archipelago. We examine a complex polygenetic paleosol on Gran Canaria that was preserved by a basaltic lava flow during the lower to middle Pleistocene. Based on a number of geochemical and mineralogical analyses of different secondary soil products and allochthonous inputs, we identify different soil-

https://doi.org/10.1017/qua.2018.64 Published online by Cambridge University Press

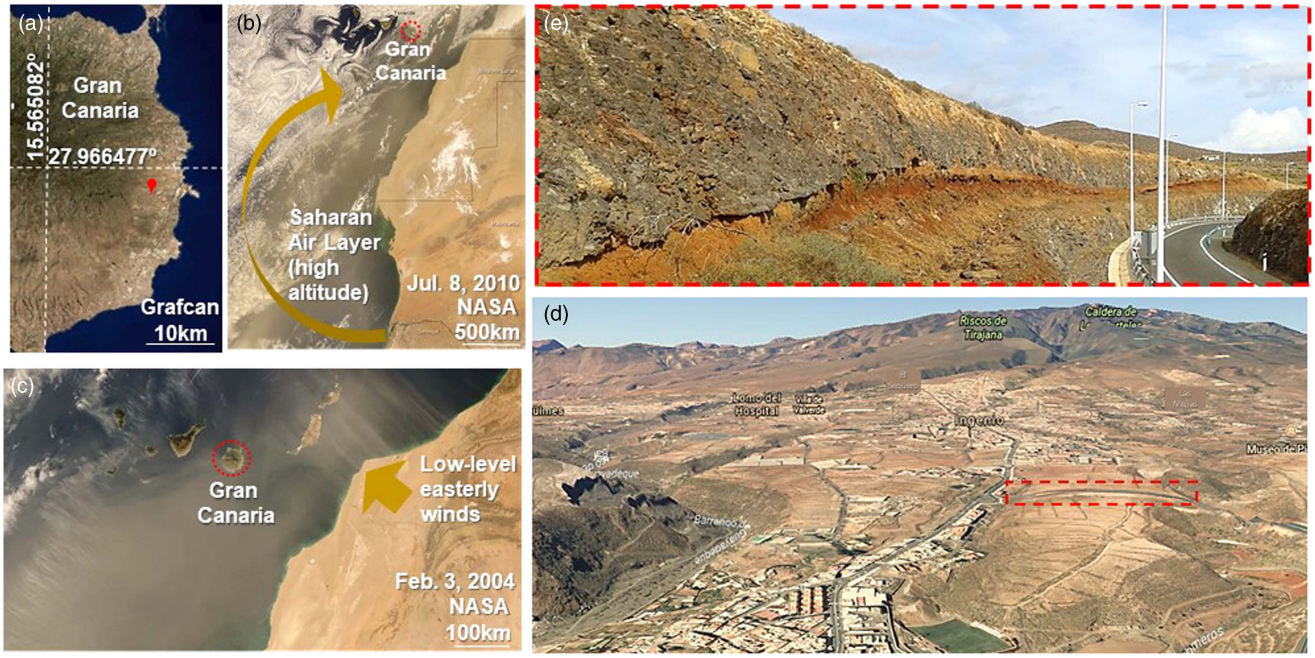

Figure 2. (a) The location of the Ingenio paleosol in Gran Canaria. (b) Typical Saharan plume dust in summer conditions. (c) Typical Saharan plume dust in winter conditions. (d) Oblique Google image of the Ingenio paleosol. The outcrop is marked in red dots. (e) A photograph of the Ingenio paleosol outcrop. (For interpretation of the references to color in this figure legend, the reader is referred to the web version of this article.)

formation processes and assess the quantity of Saharan dust input together with its implications for soil-profile development.

Study area

Gran Canaria is located off the west coast of North Africa (Fig. 2b) and is consequently affected by the sediment fluxes from the Sahara, which is a major source of natural mineral particles (NMP). On average, the island is impacted 30% of the time by Saharan dust (Criado and Dorta, 2003). These dust events are known locally as "calima" and usually last from 3 to 5 days (http://www.calima.ws/). The annual deposition rate of Saharan dust in this region is 15.6 g/m^2 (Prospero, 1996; Goudie and Middleton, 2001). The mean grain size of dust particles on Gran Canaria is about 15 µm, but ~20% are <5 µm (Menéndez et al., 2009b). High pressure at high altitude over the Sahara in the summer leads to the deflection of Saharan dust in a hook-shaped transport pathway towards the Canary Islands (Fig. 2b; Faust et al., 2015). The Saharan Air Layer (SAL) simultaneously moves towards higher "subtropical" latitudes (15–30ºN; Engelstaedter et al., 2006; Sunnu et al., 2008; Rodriguez et al., 2011). Likewise, the easterly and low-level winds carrying warm-dry air masses from the Saharan Desert during the summer are due to low Saharan thermal pressures (Fig. 2b). In contrast, during winter (Fig. 2c), calima winds blow out of thermal, low-level, high-pressure cells located over the Western Sahara towards the Atlantic Ocean. These winds are often linked to low-pressure cells close to the Canary Islands. This is reinforced by high thermal pressures over central and western Europe because, on the southern edge of those high pressures, a wind flow from east to west can be generated, crossing over the northern part of the Saharan Desert and dragging the Saharan dust towards the Canary Islands (Dorta, 1999; Menéndez et al., 2017). During these events, dust is transported towards the Canary Islands generally at altitudes <2000 m above sea level (asl).

The Canary Islands are a geologic hotspot-derived intraplate archipelago settled over Jurassic oceanic lithosphere (Schmincke and Sumita, 2010). The silica sub-saturated nature (a feature of any oceanic intraplate island) of the alkaline volcanic rocks in Gran Canaria precludes the presence of quartz in their paragenesis. Hence, any quartz particles found in any natural deposits on this land must have been transported from outside of the Canary Islands. The subaerial growth of Gran Canaria is characterized by a succession of two main magmatic phases (the shield building and rejuvenation stages), separated by an erosional gap between 8.5 and 5.3 Ma. The rejuvenated volcanism was comprised of three main phases: (1) Roque Nublo; (2) Post-Roque Nublo; and (3) recent volcanism and mainly focused in the northern sector of the island. The Roque Nublo volcanism (5.3–2.7 Ma) corresponded to the evolution of a complex stratovolcano in the central area of the island (Carracedo et al., 2002). The Post-Roque Nublo volcanism (3.5–1.5 Ma) was characterized by Strombolian activity from vents aligned with a northwest-southeast rift, with the emission of basaltic lava flows, forming the so-called "platform forming lavas" (Balcells et al., 1992). Finally, the most recent volcanism (<1 Ma) involved spatially and temporally dispersed

https://doi.org/10.1017/qua.2018.64 Published online by Cambridge University Press

Strombolian and phreatomagmatic eruptions of highly alkaline magmas over the northern sector of the island (Mangas et al., 2002).

Little information exists regarding climate conditions on Gran Canaria during the early and middle Pleistocene. For instance, warm marine fauna were found in deposits from Agaete, Gran Canaria, and attributed to the early Pleistocene (interglacial MIS 63; Meco et al., 2002). These deposits represent the upper limit of the Gelasian Stage. A continuous dust layer was deposited during the early/middle Pleistocene in a valley close by Femés (Lanzarote Island). The dust-accumulation rate in that case, however, was lower than the average accumulation rate calculated for the last 1.0 Ma (Suchodoletz et al., 2009a).

METHODOLOGY

According to field observation, Ingenio paleosol indicates a lateral extension of about 20 km² (Fig. 2 and 3). Information regarding the time period of soil formation has been provided by Guillou et al. (2004) and points towards a maximum duration of 840 ka between 2.3 ± 0.05 and 1.46 ± 0.03 Ma during the early Pleistocene. Each layer and horizon was sampled for geochemical and mineralogical analysis. Two samples were collected in the upper part of the B horizon ($1Bt_{1\text{-}2}$), and three more in the thicker lower part of the B horizon ($2Bt_{1\text{-}3}$). Furthermore, two samples were obtained from the capping basalt flow and the underlying basaltic bedrock (Fig. 4). The colors of the samples were defined using Munsell color charts.

Grain-size analyses were carried out at the GEOGAR/IOCAG Laboratory, University of Las Palmas de Gran Canaria. Previously, sodium hexametaphosphate (0.5%; Kettler et al., 2001) was added to the soil sample as a dispersing agent in a ratio of 2:1 and then stirred for 48 hours at room temperature. Clay fractions were obtained by the Robinson pipette method, in the upper 10 cm of the water column, after 8 hours of decantation from shaking beakers. Silt, sand, and gravel fractions were collected by dry-sieving of the residue from the extraction of the clay fraction.

A total of 53 elements from the 2Bt horizon and some present-day Saharan dust collected in Gran Canaria were analyzed. Major elements (SiO_2, Al_2O_3, Fe_2O_3, TiO_2, K_2O, MgO, Na_2O, CaO, P_2O_5, and MnO) were analyzed by fusion inductively coupled plasma mass spectrometry (ICP-MS), organic content was analyzed by loss on ignition (LOI), and Ba, Be, Sc, Sr, V, Y, and Zr trace elements were analyzed by fusion ICP-MS; Ag, Bi, Ce, Co, Cr, Cs, Cu, Dy, Er, Eu, Ga, Gd, Ge, Hf, Ho, In, La, Lu, Mo, Ni, Pb, Pr, Rb, Sb, Sm, Tb, Th, Tl, Tm, U, W, Yb, and Zn elements were analyzed by FUS-MS; As, Au, Br, Hg, Ir, Sc, Se, and W elements were analyzed by total digestion ICP-MS; and Cd, S by instrumental neutron activation analysis (INAA). All of these analyses were performed at the ACTLABS Activation Laboratories Ltd., Ontario (Canada), with a Perkin Elmer Sciex Elan 6100 for fusion ICP-MS analysis and a Canberra Lynx Multi Channel AnalyzermOrtec GE Detector for INAA. Major element detection limits range from 0.01 to 0.1 wt% and trace element detection limits range from 0.01 to 1 ppm, except those for gold (Au) and iridium (Ir), expressed in ppb, with a detection limit of 1 ppb. Bi, In, Au, Br, Hg, and Ir concentrations fell below detection limits.

Mineral determination of all samples was made by analyzing thin sections using a petrographic microscope (Leitz Orthoplan) at the GEOGAR/IOCAG Laboratory, University of Las Palmas de Gran Canaria. The X-ray diffraction, scanning electron microscopy with energy-dispersive X-ray spectroscopy (SEM-EDX) analyses were performed at the Unitat de Microscòpia Electrònica de Rastreig, Universitat de Barcelona. Complementary method for mineral determination was X-ray powder diffraction (XRPD), that

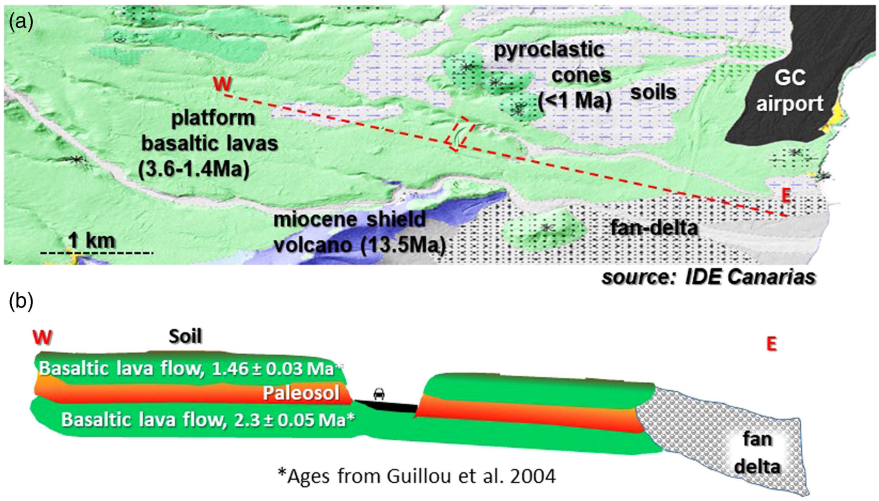

Figure 3. (a) The geological map of the study area (IDE Canarias, http://visor.grafcan.es/dgse/). (b) West-east cross section of the Ingenio paleosol, marked in the dashed red line. (For interpretation of the references to color in this figure legend, the reader is referred to the web version of this article.)

https://doi.org/10.1017/qua.2018.64 Published online by Cambridge University Press

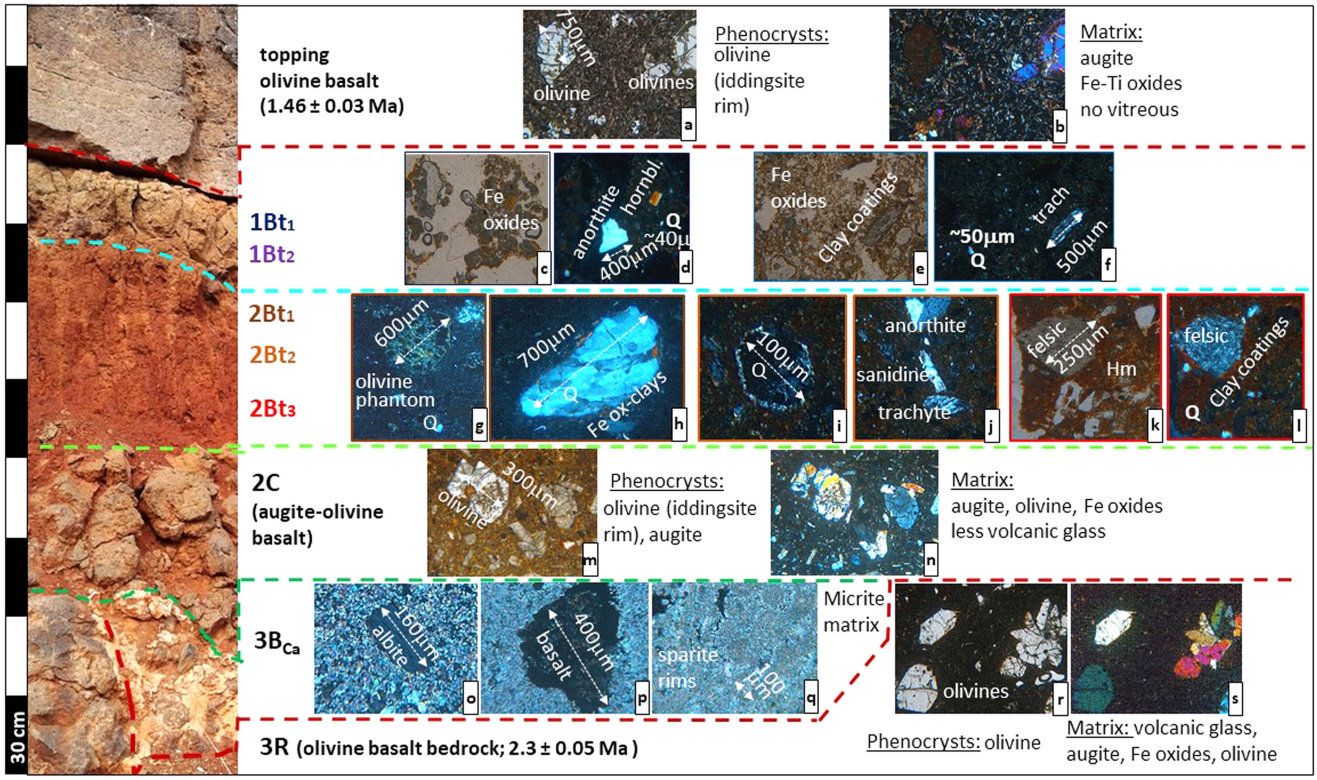

Figure 4. (color online) The column section of the Ingenio paleosol, showing some examples of the texture and minerals identified in the thin-section images.

was conducted at the Unitat de Microscòpia Electrònica de Rastreig, University of Barcelona. Data were collected with a Panalytical X'Pert PRO MPD X-ray diffractometer with monochromatized incident Cu Kα1 radiation at 45 kV and 40 mA, and equipped with a PS detector with amplitude of 2.113°. The patterns were obtained by scanning random powders from 4° to 80° (2θ) on samples crushed in an agate mortar to a particle size below 40 µm. Data sets were obtained by a scan time of 50 seconds at a step size of 0.017° (2θ) and variable divergence slit. Mineral identification and semi-quantitative results were facilitated using the X'Pert search-match software with Powder Diffraction File, version 2 from JCPDS. When quartz was present in the sample, it was used as an internal standard to correct diffraction patterns for instrumental shifts in (2θ) position. Quantitative mineral phase analyses were obtained by full refinement profile. The software used was TOPAS V4.2.

Fe-oxides were measured at the Department of Agronomy Laboratory, University of Córdoba. Three types of Fe-oxides were sequentially extracted, the first being ferrihydrite (Fh). The sample was dissolved in acid ammonium oxalate using the Schwertmann (1964) method (Fe_0). Secondly, Mgh from the Fe was extracted using sulfuric acid (Fe_s); and thirdly, the Fe in Hm plus Gt was extracted using sodium dithionite in a hot (75ºC) sodium citrate and sodium bicarbonate solution (Fe_d; Mehra and Jackson, 1958). If we assign Fe_d to the combination of Fe in stoichiometric Hm (Fe_2O_3) and Gt (FeOOH), we can estimate the Gt content as follows (Scheinost et al., 1998):

$$Gt = 1.59 \times (Fe_d - Hm / 1.43) \quad [1]$$

To solve this equation, it is necessary to use the diffuse reflectance spectra technique (DRS; Scheinost et al., 1998; Torrent and Barrón, 2002; Torrent et al., 2007). The DRS is a precise and non-destructive method to quantify soil properties. The DRS can detect the presence of either Hm or Gt at <0.1% in mixtures with other soil minerals. The DRS spectra of the Bt samples was recorded at a scan rate of 30 nm/min from 380 to 770 nm in 0.5-nm steps using a Varian Cary 5000 UV-Vis-NIR spectrophotometer equipped with a diffuse reflectance attachment. From the calculation of the second derivative amplitude peaks in the Kubelka-Munk function (A_{Gt} and A_{Hm}), it is possible to estimate the relation between Hm and Gt. According to Scheinost et al. (1998), to complete the calculation of Hm and Gt contents, the following equation can be used:

$$Hm / (Hm + Gt) = -0.068 + 1.325\ [A_{Hm} / (A_{Hm} + A_{Gt})] \quad [2]$$

The iron concentration in all extracts was determined by Atomic Absorption Spectroscopy (AAS) using a Perkin-Elmer 420 instrument. The total Fe content (Fe_t), expressed as an ion weight percentage, was calculated from the Fe_2O_3 weight percentage.

The extent of weathering for Bt and current dust was quantified by the chemical index of alteration (CIA), with

https://doi.org/10.1017/qua.2018.64 Published online by Cambridge University Press

high values denoting more intense weathering (Nesbitt and Young, 1989; McLennan et al., 1993; Price and Velbel, 2003):

$$CIA = [Al_2O_3 / (Al_2O_3 + K_2O + Na_2O + CaO)] \times 100 \quad [3]$$

where major element oxides are divided by their molar mass. The CaO represents calcium in the silicate fraction. The Bt horizon is carbonate free, but the current dust has a carbonate content of about 20%. In the latter case, $CaO_{silicate}$ was calculated as:

$$CaO_{silicate} = (CaO_{total} - CaCO_3) \times 56.1 / 100.1 \quad [4]$$

where 56.1 and 100.1 are the relative molar weights of CaO and $CaCO0_3$, respectively.

RESULTS

This paleosol is located at the excavation of the Carrizal-Ingenio ring road inaugurated in 2007 (X, 458.568; Y, 43.088.062; Z, 180 m asl; Fig.2). The outcrop is 0.5 km long and the visible extension of the paleosol in the field and satellite image is about 20 km^2. The paleosol developed on a basaltic lava that has a presumed age of 2.3 ± 0.05 Ma (rejuvenation stage of the island), and the paleosol was covered by a later basaltic lava flow dated to 1.46 ± 0.03 Ma (Fig. 3; Guillou et al., 2004). This results in a maximum time period for profile development of ~840 ka during the Gelasian and Calabrian stages. This profile is a complex sandwiched paleosol, developed on a basaltic platform originating from the rejuvenation stage of the island (Fig. 3). The underlying bedrock consists of olivinic basalt, with iddingsite rims on the olivine phenocrysts, and a matrix of volcanic glass, augite, Fe-oxides, and olivine (3R; Fig. 4). A petrocalcic horizon forms the first layer of this paleosol, infilling and expanding on the bedrock ($3B_{Ca}$). The calcification features, in the form of micritic infillings, were fragmented, dissolved, and covered by sparitic infillings. Phenocryst phases in this petrocalcic horizon are, aside from calcite, minerals such as plagioclase and basaltic rock fragments. On top of the B_{Ca} horizon there is some weathered basaltic lava (2C), with a different composition from the olivine basaltic bedrock, and it can be classified as an augitic olivine-basalt,

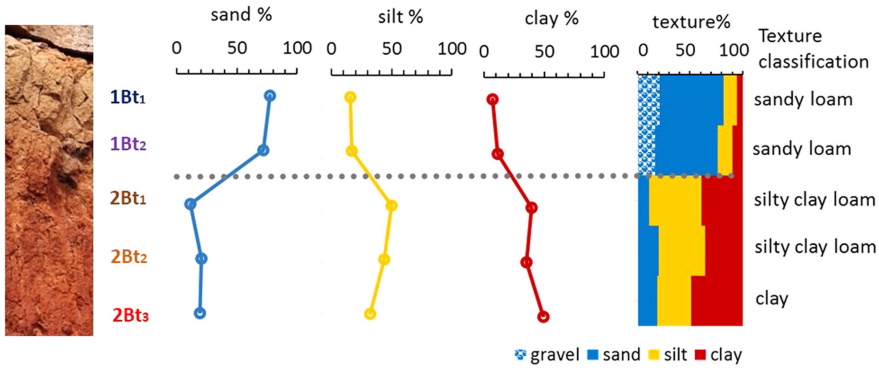

Figure 5. (color online) Bar-and-whisker plots showing the sand-silt-clay percentages and the texture classification of each sample from the Bt horizons of the Ingenio paleosol profile. The grey dot line represents the stone-line.

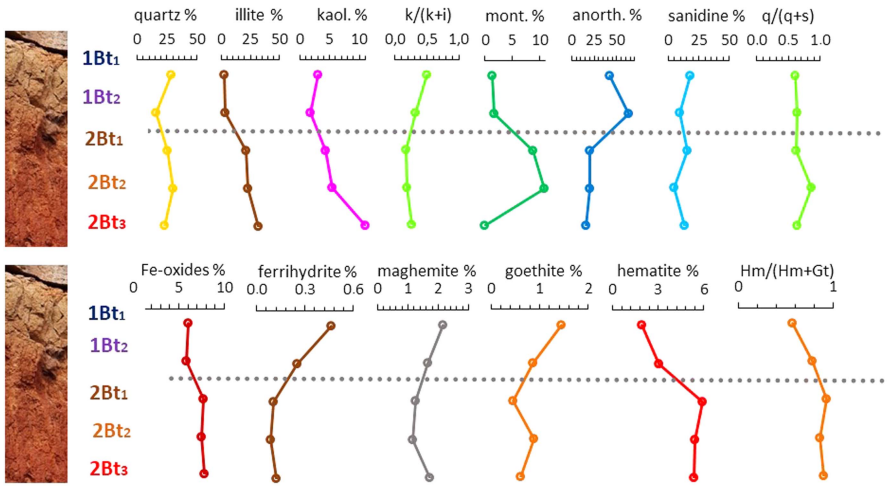

Figure 6. (color online) Bar-and-whisker plots showing the main mineral composition, the kaolinite versus illite (k / [k + i]), quartz versus anidine (q / [q + s]), and the hematite versus goethite (Hm / [Hm + Gt]) ratios, from the Bt horizons of the Ingenio paleosol. The grey dotted line symbolizes the stone-line.

https://doi.org/10.1017/qua.2018.64 Published online by Cambridge University Press

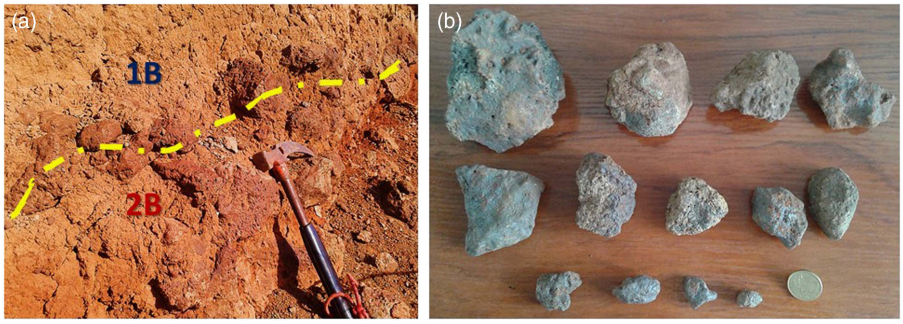

Figure 7. (color online) (a) A photograph of the stone-line of the Ingenio Paleosol. (b) Some examples of rounded- and kidney-shaped gravels from the stone-line in which iron coatings can be observed.

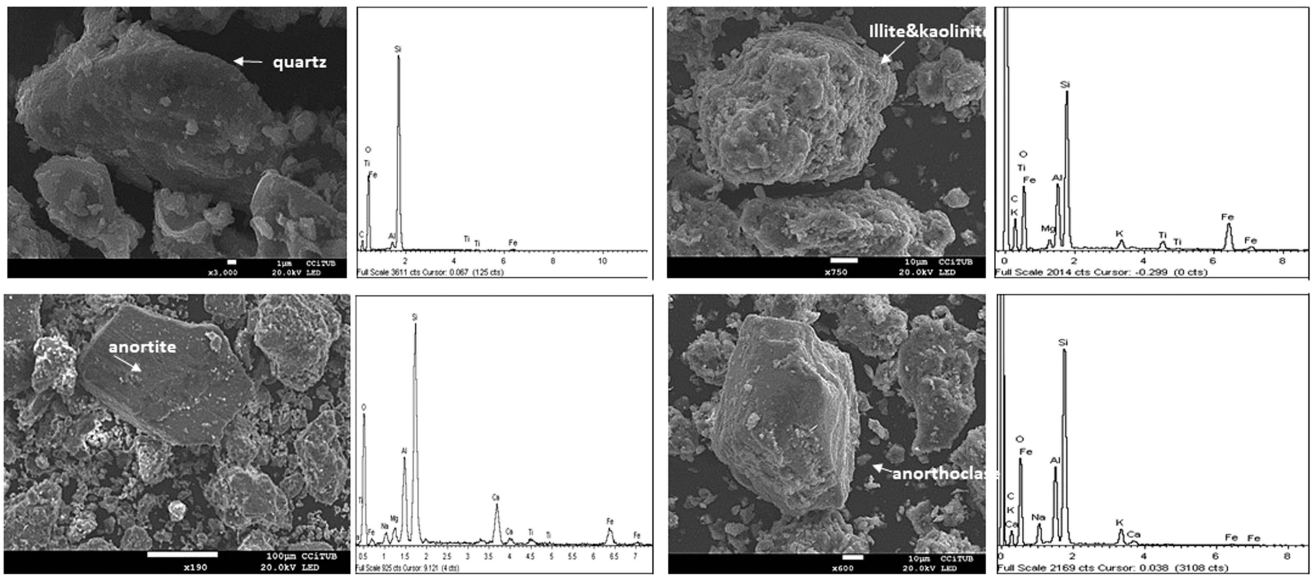

Figure 8. Scanning electron microscopy (SEM) images of the main minerals identified in the Bt horizons of the Ingenio paleosol profile.

with phenocrysts of olivine-augite and a matrix of augite, olivine, Fe-oxides, and less volcanic glass than 3R. The following layers are two textural B-horizons ($1Bt_{1\text{-}2}$ and $2Bt_{1\text{-}3}$; Fig. 4), which have a distinctive color and a discontinuous basalt stone line between them. The $1Bt_{1\text{-}2}$, horizon is strong brown (7.5YR 5/6), and the $2Bt_{1\text{-}3}$ horizon is red (10R 4/8-6; $2Bt_{1\text{-}3}$, Fig. 4). Textural horizons were characterized by illuviated clays, observed both in the field and under the microscope. The basaltic bedrock weathering products observed in Bt horizons, the sand and gravel content (Fig. 5), and the presence of aeolian quartz (from the Saharan dust; Fig. 6) suggest that $1Bt_{1\text{-}2}$ is also comprised of relocated slope deposits. The stone line consists of rounded gravel and cobbles with black-reddish clayey-Fe coatings (Fig. 7). The $1Bt_{1\text{-}2}$ horizon has hardened. Higher Fe-oxides content (7.5–7.8 versus 6.0–5.8%), and more hematite (5.3–5.9 versus 1.9–3.1%) in $2Bt_{1\text{-}3a}$ account for the color differences of those Bt horizons. The hematite versus hematite and goethite ratio, Hm / (Gt + Hm), is also higher in $2Bt_{1\text{-}3}$ (0.9 versus 0.6–0.8). More differences in mineralogy were obtained between those Bt horizons: $2Bt_{1\text{-}3}$ revealed more quartz (23–30 versus 16–28% in 1Bt1-2), more kaolinite (6–11 versus 2–4% in 1Bt1-2), more illite (21–32 versus 3–4%), and more montmorillonite (9–11 versus 1–2% in 1Bt1-2), but less sanidine (5–16 versus 9–18%), and less anorthite (16–20 versus 62–64% in 1Bt1-2; Fig. 6–8).

The total geochemical composition of $2Bt_{1\text{-}3}$ and current Saharan dust is shown in Figure 9. Most of the elements analyzed (34 of 53) were more abundant, a two- to three-fold increase, in the paleosol. Besides this difference, the concentrations of CaO, Na_2O, Sr, P_2O_5, Zn, Sb, and Mo were double that $2Bt_{1\text{-}3}$ in the current dust. The levels of Si, K_2O, MgO, Ba, Mn, Cu, Y, Sn, Cs and U, aside from LOI, however, remained constant in both samples. The REE concentration was significantly higher (about twice; Fig. 10) in the paleosol than in the present-day Saharan dust. The geochemical index of weathering (CIA) for $2Bt_{1\text{-}3}$ was 80, whereas for the Saharan dust it was 43.

DISCUSSION

Paleosol classification

We used the property-based paleosol classification system linked to genetic processes proposed by Nettleton et al. (2000). This is based on enduring properties such as

https://doi.org/10.1017/qua.2018.64 Published online by Cambridge University Press

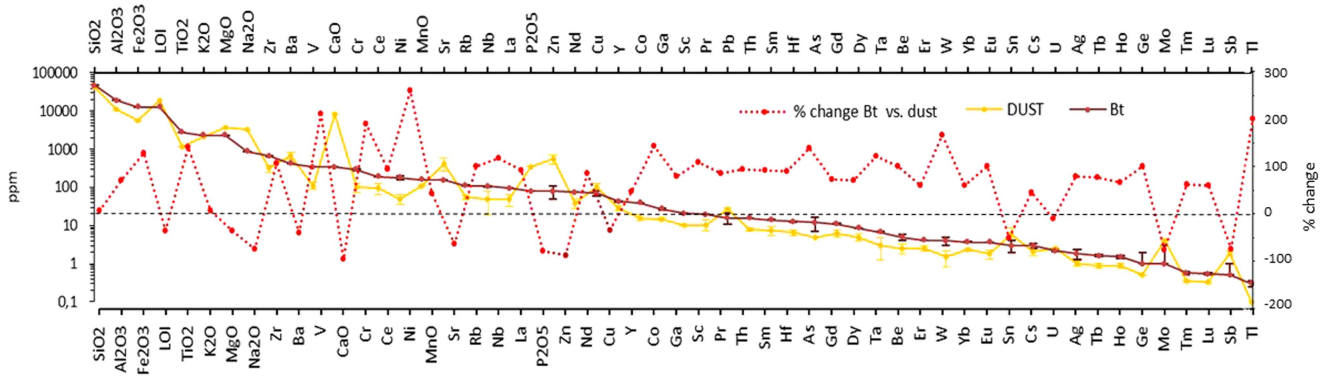

Figure 9. Geochemical composition of the 2Bt horizon from the Ingenio paleosol, the present-day Sahara dust collected in Gran Canaria. The red dashed line is the percentage change of the elemental ratio between elements in the Bt horizon and in the Saharan dust (% change of ratios = 100 [(R_{Bt} - R_{dust}) / R_{dust}]). The chemical elements are ordered accordingly to their abundance. (For interpretation of the references to color in this figure legend, the reader is referred to the web version of this article.)

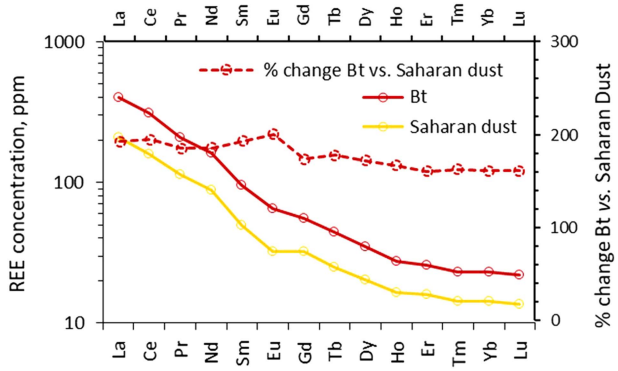

Figure 10. Chondrite normalization of the rare earth elements (REE) concentration, in ppm, of the Ingenio paleosol and the present-day Saharan dust samples collected on Gran Canaria. The red dashed line is the percentage change of the elemental ratio between such element in the Bt horizon and in the Saharan dust (% change of ratios = 100 [(R_{Bt} - R_{dust}) / R_{dust}]). (For interpretation of the references to color in this figure legend, the reader is referred to the web version of this article.)

horizonation, soil fabric, root and worm casts, redoximorphic features, the proportion of resistant minerals, and the degree of mineral weathering.

The Ingenio profile was truncated, having lost all or part of the upper horizons. The lower ones were preserved due to the basaltic flow covering them. This paleosol has over 10% weatherable minerals in the sand-silt fractions (i.e., anorthite and sanidine). The clay mineral suite is dominated by illite, kaolinite, and montmorillonite in the Bt horizons, which are also accumulatively formed by volcanic minerals (e.g., anorthite), Saharan dust (e.g., quartz), and local minerals (e.g., sanidine). Accurately measuring a total extension of this paleosol is not possible, but it covers at least 20 km^2. The paleosol has textural horizons and abundant Fe-oxides (6–8%). Although this paleosol has both volcanic bedrock and textural horizons with clay skins, required for Paleoandisol and Paleoeldisol definitions, respectively, it also has a petrocalcic horizon. This classification system (Nettleton et al., 2000) places all paleosols with petrocalcic horizons in the Paleoaridisol order, prioritizing this feature above the previous ones. Consequently, our final classification of the Ingenio complex paleosol describes it as accretionary, oxidized, truncated, carbonate-enriched, Krypt Paleoaridisol, and aeolian/pyroclastic.

The Ingenio profile is a buried paleosol largely preserved because of burial, but post-burial changes and alteration such as oxidation and loss of organic matter have occurred (Olson and Nettleton, 1998). Moreover, the paleosol is a relict and polygenetic and, by definition, has persisted through a number of climatic cycles. We agree with Nettleton et al. (2000) about the dilemma that occurs in matching morphological features to cycles, the concern about if one of the cycles had a dominant influence on paleosol development, and if the inherited features that we see and describe originate in the dominant cycle or a combination of all cycles.

We suggest that the Ingenio paleosol could reflect different paleoenvironmental conditions that may be linked to several climatic cycles: soil formation (Bt horizons) linked to biostatic (Erhart, 1955) wetter periods and soil erosion (stone-line formation) linked to rhexistasic drier and more contrasted periods. The calcic material in-between the basaltic bedrock (B_{Ca}) likely formed earlier in the course of basalt weathering and is decoupled from the formation of the overlying Bt material. Since we interpret the B_{Ca} as an older formation that preceded the formation of the $2Bt_{1-3}$, all sub- and topsoil horizons that belonged to the B_{Ca} (and that were formed during a biostatic period that was more contrasted than Bt-formation periods) ought to have been completely eroded in a subsequent rhexistasic period. Aridity regimes are normally associated with more soil erosion and, consequently, more clays (such as kaolinite) are found in oceanic sediment records (Ehrmann et al., 2017). Furthermore, the capping basaltic flow would have formed during or shortly after a biostatic wet-warm period (interglacial 47 MIS; Fig. 1), which could, in part, have protected the paleosol from erosion. B_{Ca} could have been partially dissolved during

https://doi.org/10.1017/qua.2018.64 Published online by Cambridge University Press

biostatic periods, however, and the current B_{Ca} might be the remains of the original one.

Stone-line and erosion facts

Stone lines, or stone layers, have been accounted for in three different ways (Goudie, 2013). (1) They can be the results of residual surface accumulations (paleo-pavements), which were later covered by colluvial-like finer sediments. Such a stone line might represent drier cool conditions (Runge, 2001). (2) They can be parts of paleo-channels that were formed by the redistribution and concentration of gravel by surface water flows and related colluvial activity. (3) They can be the result of bioturbation by termites, ants, worms, and even roots (Wilkinson et al., 2009). This selective zoogenic uptake of fine material in a soil could lead to a concentration of coarser material at lower depths.

Stone lines may well be the result of abrupt truncation in soils. Apart from this, the covering material raises questions about its autochthonous versus allochthonous origin (Johnson et al., 2005; Morrás et al., 2006; Fedoroff et al., 2010). Without going into what type of material covers the stone line, we hypothesize that two periods of pedogenic occurred at the Ingenio profile, in two biostatic phases ($1Bt_{1\text{-}2}$ and $2Bt_{1\text{-}3}$) separated by a possible rhexistasic episode (stone line) as well as continuous aeolian input from local and Saharan sources. The suggestion concerning aeolian input is based on the pervasive presence of minerals and rock fragments that do not originate from the basaltic bedrock (e.g., quartz, sanidine, and felsic rocks fragments; see Fig. 4). Previous work showed that the presence of quartz in Canarian soils is the result of the input of Saharan dust (Menéndez et al., 2007; Suchodoletz et al., 2013).

Stone-line formation is significant in tropical geomorphology because it shows that there is relative landscape stability with ongoing moderate erosion but also that a contemporary interfluvial position might have once occupied a lower landscape position (Brown et al., 2004). The Ingenio profile is located in an interfluvial position, surrounded to the west by the well-developed Guayadeque ravine and to the north by the Los Romeros tributary (Fig. 2d). The capping basalt covers a wavy surface sloping down seawards, however, which could be the result of incipient fluvial-colluvial erosion.

In summary, we do not reject the possibility of the three stone-line interpretations in unison for the Ingenio profile, assuming that they might not be mutually exclusive. Firstly, and perhaps the most likely, the stone line could mark some selective soil erosion due to aridification conditions (case 1). Secondly, despite the fact that the Ingenio profile is currently in an interfluvial position, the stone line could be linked to fluvial-colluvial activity (case 2). Finally, the covering material may be autochthonous, as it has minerals in it that are different from the bedrock (quartz, sanidine, and trachytic fragments from colluvial-aeolic sources). Nonetheless, it contains an edaphic imprint (case 3).

We also tried to compare it to modern conditions for a more thorough interpretation of the Ingenio profile. Since the earliest human occupation of Gran Canaria, around the third to fourth centuries BC, however, extensive deforestation has led to strong and widespread soil erosion. Erosion was accelerated with the occupation of the island by the Spanish Royal Crown at the end of the fifteenth century (Morales et al., 2009). This has brought about the arid character of nearly the whole surface of Gran Canaria today, most of the soils of the island being deforested, truncated, and in non-equilibrium with their edaphic secondary products (Fe-oxides and clays). In addition, the considerable impact of human activity on this limited territory makes it difficult to compare the current environment and its associated climatic conditions with other environmental and climatic conditions in the past.

Geochemistry and weathering intensity

Higher REE concentration in soils was found to be linked to secondary phosphates (Sadeghi et al., 2013). Industrial activities in northwest Africa seem to be the main contributors of the phosphate content in the Saharan dust that reaches the Canary Islands (Rodriguez et al., 2011). REE content in the Ingenio paleosol, however, is double that in the current aeolian Saharan dust, while the phosphorous content is 75% higher (Fig. 9 and 10). This could mean that the aeolian Saharan dust in Gran Canaria does not increase the amount of REE in soils, but improves the soil nutrition, as was determined in La Palma Island (Suchodoletz et al., 2013).

The geochemical index of weathering for the $2Bt_{1\text{-}3}$ (CIA = 80) was in the range of laterites measured in China (CIA = 79–88; Zhao et al., 2017), where it was interpreted as a strong chemical weathering process. The present-day dust (CIA = 43), however, showed a markedly lower value. Consequently, the high CIA value of the Ingenio paleosol cannot be caused by the Saharan aeolian input alone. Clay mineral assemblages also provide information about weathering intensity that should help to better characterize the Ingenio profile.

The amount of kaolinite in Saharan dust ranges from 0 to 8% (Scheuvens et al., 2013). In present-day Gran Canarian soils, it is about $0.2 \pm 0.3\%$ (Menéndez et al., 2007), while the kaolinite content in the Ingenio paleosol is higher (2–11%). These results could mean that the kaolinite in the paleosol was mainly formed *in situ*, or that the amount of kaolinite in early Pleistocene dust was greater than in the present-day dust. Kaolinite found in Bt horizons is a common pedogenic clay mineral formed as the end-product of intense *in-situ* chemical weathering under hot-moist climate conditions (Chamley, 1989; Hong et al., 2010). In contrast, the predominance of illite is characteristic of cooler-drier climates, with lower weathering rates (Hallam et al., 1991; Hong et al., 2013). Another clay mineral found at the Ingenio profile, montmorillonite, is known to be formed in poorly drained

https://doi.org/10.1017/qua.2018.64 Published online by Cambridge University Press

soils of tropical or subtropical regions subject to strongly seasonal rainfall (Chamley, 1989).

The clay content in $1Bt_{1-2}$ is lower than in the $2Bt_{1-3}$ (7–1% versus 36–49%; Fig. 5). However, the kaolinite / (illite + kaolinite) ratio in $1Bt_{1-2}$ is higher than in $2Bt_{1-3}$ (0.3–0.5% versus 0.2–0.3%). This ratio could reflect more weathering intensity in $1Bt_{1-2}$.

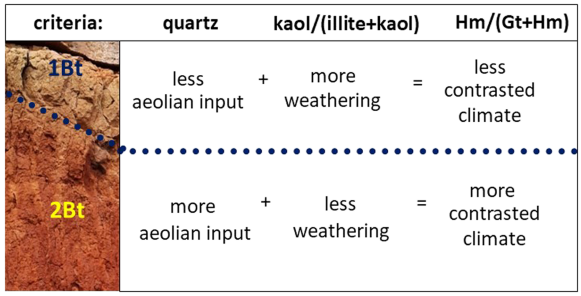

Figure 11. (color online) Conceptual formula of the climatic oscillations during the lower Pleistocene based on the aeolian input (quartz), the intensity of weathering (kaolinite versus illite ratio), and the contrasted climate conditions (hematite versus goethite ratio) from the Bt horizons of the Ingenio paleosol. Further details in the text.

Iron Oxides

The Fe-oxide content in Saharan dust is about 4% (Lafon et al., 2004), which is a lower proportion than the Fe-oxides from Bt horizons in the Ingenio paleolosol (6–8%). This suggests that aeolian inputs have been limited but not negligible and, as Figure 6 suggests, with the presence of quartz and new hematite formed in the paleosol. In addition, Saharan dust contains fewer minerals that will produce Fe-oxides through weathering in comparison with the basalt bedrock below the paleosol. Conversely, the fact that the $1Bt_{1-2}$ has a lower Hm / (Hm + Gt) ratio than the $2Bt_{1-3}$ is coherent with two hypotheses: (a) a $1Bt_{1-3}$ pedogenesis in a more humid and less seasonally contrasted environment, or/and (b) a lower dust content. The latter hypothesis is partly supported by the statement that the quartz content as well as the Hm / (Hm + Gt) ratio decrease from $2Bt_{1-3}$ to $1Bt_{1-2}$ (Fig. 6). On the other hand, the circumstance that the Hm / (Hm + Gt) ratio decreases substantially from $2Bt_{1-3}$ to $1Bt_{1-2}$ is also compatible with the first hypothesis.

Hematite is the main Fe-oxide at the Ingenio profile. The presence of hematite in the Bt horizons in large amounts (2–6%) implies weathering under warm and seasonally dry climatic conditions during the formation of this horizon. The Hm / (Gt + Hm) ratio increases with the intensification of alternating wet and dry environmental conditions and mild and hot temperatures (Cornell and Schwertmann, 2003; Torrent et al., 2007; Zhao et al., 2017). Since the Hm / (Gt + Hm) ratio in $1Bt_{1-2}$ is lower than in $2Bt_{1-3}$, and based on the assumption that the Fe-oxides indicate *in-situ* weathering conditions, the upper Bt horizon should reflect a moister and less-contrasted regime. Zhao et al. (2017) found that the correlation between Hm / (Hm + Gt) and kaolinite was weak. The same tendency was observed between kaolinite / (illite + kaolinite) and Hm / (Hm + Gt) ratios at the Ingenio profile (Fig. 6).

The Hm / (Gt + Hm) ratio at the Ingenio profile (0.82 ± 0.13) is almost twice than that from the current Saharan dust collected on Gran Canaria (0.47 ± 0.12; Lázaro et al., 2008). Assuming that the hematite proportion in the Saharan paleo-dust is similar to the present Saharan dust, a major *in-situ* edaphic hematite formation at Ingenio paleosol could reflect that there was less aridity during the early Pleistocene than at present (Yang et al., 2006; Zeng et al., 2017; Zhao et al., 2017).

Aeolian accumulation on the Ingenio paleosol

Two distinctive mineral sources can be attributed to aeolian input at the Ingenio paleosol: long-distance Saharan provenance for quartz, and local for sanidine. These two minerals could be used to measure the autochthonous and allochthonous accumulation rate (quartz versus sanidine, q / [q + s]; Fig. 6). This rate was the same throughout the profile (0.6), but higher in $2Bt_2$ (0.9). Our interpretation is that the Saharan versus local input might have been equal during the development of the paleosol, except for during the $2Bt_2$ formation when Saharan dust might have been increased or the local input decreased.

The existence of quartz in the Bt horizons could be the consequence of continuous aeolian input during their formation, provided that lateral supply due to slope processes can be ruled out. This aeolian material may be produced either by the seasonal wet-dry conditions in Gran Canaria or by the dry-dusty conditions in the Sahara, as happens at present (Fig. 2b and c). The increase in quartz through the profile may possibly be due to a rise in Saharan dust input and/or reinforced by soil weathering. This weathering could reduce the concentration of the more labile primary minerals (feldspars) and, consequently, might increase the proportion of the more resistant ones, such as quartz. Gathering now previous interpretations we suggest that: (1) there was less aeolian input during the formation of 1Bt than 2Bt (quartz proportion is lower in 1Bt, 16–28% than in 2Bt, 23–30 %); (2) the climate was less contrasted during the formation of 1Bt than 2Bt ([Hm / (Gt + Hm)] ratio is 0.6–0.8 in 1Bt and 0.9 in 2Bt samples); and (3) weathering was more intense in 1Bt than in 2Bt (kaolinite vs. illite ratio is higher in 1Bt, 0.3–0.5, than in 2Bt, 0.2–0.3; Fig. 11).

Two loess-like silty deposits were identified in Gran Canaria (Jinámar and Gáldar profiles; Menéndez et al., 2009a) with ages of 1.96–0.01 Ma (Pleistocene) and <0.4 Ma (middle Pleistocene to late Quaternary). Dating of those loess-like deposits is wide-ranging, although it is highly probable that the Jinámar profile started its formation earlier than the Gáldar profile, since there was a time lag of 1.56 Ma (63% of the Pleistocene) between them. Those deposits showed a mean quartz content of 49 and 79%, respectively. The mean quartz content of the Ingenio

https://doi.org/10.1017/qua.2018.64 Published online by Cambridge University Press

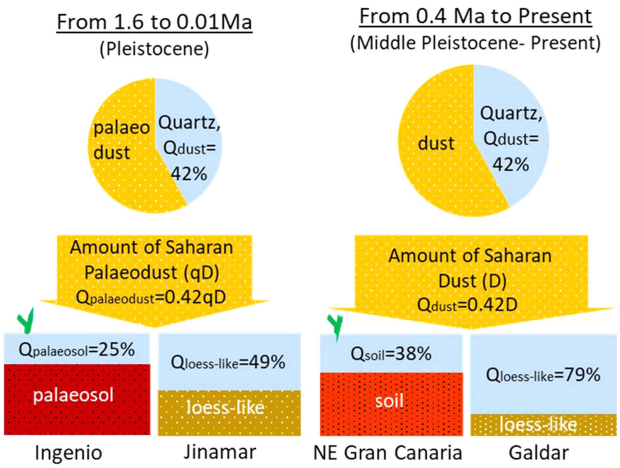

Figure 12. (color online) Reconstruction of the hypothetical Saharan paleodust amount regarding the actual Saharan dust collected in Gran Canaria. Calculations are based on the quartz percentage in northeast Gran Canaria soils, the Ingenio paleosol of this study, and two loess-likes of Gran Canaria (Jinamar and Galdar). Further details in the text.

paleosol and in Holocene Gran Canarian soils was on average 25 and 38%, respectively (Menéndez et al., 2007), which could be defined as $Q_{paleosol}$ and Q_{soil}. Assuming that the 42% of quartz content in Saharan dust remains constant at Gran Canaria over time (Fig. 12; Menéndez et al., 2007), the amount of hypothetical Pleistocene Saharan dust (qD) relative to the present amount (D) could be estimated. Hence, the amount of present Saharan dust (D) and quartz content (Q_{dust}) are related as:

$$Q_{dust} = 0.42\,D \quad [5]$$

Additionally, the amount of a Pleistocene Saharan dust (qD) and quartz content (Q_{dust}) relationship would be:

$$Q_{paleodust} = 0.42\,qD \quad [6]$$

Where q is a change factor of the amount of Saharan paleo-dust regarding Saharan dust.

Concerning soil and paleosol dust input, another assumption is that quartz contents remained constant for calculating dust amounts:

$$Q_{dust} / Q_{soil} = Q_{paleodust} / Q_{paleosoil} = \text{constant} \quad [7]$$

Thus, q can be estimated as:

$$\left.\begin{aligned} \text{Present} &= \frac{0.38}{0.42D} \\ \text{Past} &= \frac{0.25}{0.42qD} \end{aligned}\right\} \begin{aligned} &\frac{0.38}{0.42D} = \frac{0.25}{0.42qD} \\ &\frac{0.42qD}{0.42D} = \frac{0.25}{0.38} \\ &q = 0.66 \end{aligned} \quad [8]$$

As a result, the amount of the Saharan paleo-dust that hypothetically reached Gran Canaria would be 34% less than present Saharan dust.

In the same way, loess-like dust inputs in the Pleistocene (1.96–0.01 Ma, Jinámar) and middle to late Quaternary (<0.4 Ma, Gáldar), need a similar assumption of constant quartz contents for calculating dust amounts:

$$Q_{dust} / Q_{Galdar-loess-like} = Q_{paleodust} / Q_{Jinamar-paleosol} = \text{constant} \quad [9]$$

Thus, q can be estimated as:

$$\left.\begin{aligned} \text{Present} &= \frac{0.79}{0.42D} \\ \text{Past} &= \frac{0.49}{0.42qD} \end{aligned}\right\} \begin{aligned} &\frac{0.79}{0.42D} = \frac{0.49}{0.42qD} \\ &\frac{0.42qD}{0.42D} = \frac{0.49}{0.79} \\ &q = 0.62 \end{aligned} \quad [10]$$

As a result, the amount of the Saharan paleo-dust that hypothetically reached Gran Canaria would be 38% less the present Saharan dust. Remarkably, this result is very close to the quartz content calculated with the lineal relationship between the quartz content in those soils (33%). This difference (33–38% lower in Saharan paleo-dust) could be explained in two ways. One possibility is that the proportion of quartz in dust has changed over time (then, our first assumption should be wrong), while the other possibility is that the amount of dust that reaches Gran Canaria is higher nowadays than it was for most of the Pleistocene.

The current Saharan dust-sedimentation rate in the Canary Islands area was calculated by Prospero (1996) and Goudie and Middleton (2001) as 1.56 g/cm^2/ka. Considering this dust sedimentation rate, the maximum time span at the Ingenio paleosol (~840 ka^{-1}), the dust density (1 g/cm^3) and the fact that only 50% is finally stabilized (Cattle et al., 2002), the potential Saharan dust deposited on this profile should be about 6.6 m. Likewise, as the estimated dust deposition for the Pleistocene is 33–38% lower than measured today, the Saharan dust potentially deposited during the early Pleistocene would be about 4.4–4.5 m. Nevertheless, the Bt thickness of the Ingenio paleosol is about 1.2 m (Fig. 4). This substantial reduction in the thickness of the aeolian input could be explained by several factors: (1) subaerial erosion; (2) compaction of the Saharan dust when it becomes integrated into the soil; and (3) the pressure of the overlying basaltic flow.

A PALEOCLIMATE INTERPRETATION OF THE INGENIO PALEOSOL

Cyclical aridification of North Africa began by at least 3.8 Ma, with an increase in the severity of arid events by ~2.3–2.5 Ma (Pokras, 1989; Goudie and Middleton, 2001). This period coincided with a higher amplitude of glacial-interglacial MIS oscillation (Fig 1). Furthermore, the frequency of glacial-interglacial cycles was 2.5 times higher in the Upper Pliocene–lower Pleistocene than in the middle–upper Pleistocene, although difference between cycles was less extreme (with lower oscillations) than in the middle–upper Pleistocene owing to the less drastic glacial periods (Leroy, 2007). Meco et al. (2015) estimated the presence of the Canary Current as an eastern branch of the North Atlantic subtropical gyre between 4.2 and 2.9 Ma, based on records of tropical fauna. The appearance of this cold stream intensified the Gelasian (2.6–1.8

https://doi.org/10.1017/qua.2018.64 Published online by Cambridge University Press

Ma) cold cycles, at least regionally. The aridification of northwest Africa was probably due to the increasing strength of the trade winds (Leroy and Dupont, 1997).

The basaltic lava flow that covered the Ingenio paleosol (1.46 ± 0.03 Ma; Guillou et al., 2004), corresponds to the period of MIS 47 to 49 (Fig. 1). Despite all the uncertainties discussed earlier, we would suggest that this polygenetic paleosol could reflect at least three different climatic/environmental configurations. $1Bt_{1\text{-}2}$ and $2Bt_{1\text{-}3}$ horizons may be linked to biostatic (more moisture) periods, and a residual $3B_{Ca}$ may indicate strong erosion dynamics in the course of a rhexistasic (drier) period. The $2Bt_{1\text{-}3}$, might be consistent with more contrasted climate conditions (higher Hm / [Hm + Gt] ratio) and more aeolian input (higher quartz content). This $2Bt_{1\text{-}3}$ could have ended with the stone-line formation. The following period, $1Bt_{1\text{-}2}$, could possibly reflect the less-contrasted climate conditions (lower Hm / [Hm + Gt] values), less aeolian input (the lower quartz proportion) and more weathering intensity (the higher kaolinite / illite + kaolinite ratio). This younger horizon ($1Bt_{1\text{-}2}$) is truncated and hardened. Volcanic activity often permits the use of radiometric dating, which allows for stratigraphic hypotheses. Local volcanic activity, however, can have an effect on the local climate. The main factor that accelerates the hardening process in soil is the erosion resulting from the removal of the forest cover (Mbagwu, 2008). Thus, the hardening process of $1Bt_{1\text{-}2}$ could have been due to a regional climate aridification and/or to the local volcanic activity around MIS 47. At this point, however, we have no comprehensive explanation for this.

CONCLUSION

Although the Ingenio profile may have been influenced by a number of local and site-specific factors, we would suggest that this lower Pleistocene complex paleosol shows the imprint of at least three different climatic episodes (Fig. 11–13). The residue of the oldest one could be a petrocalcic horizon ($3B_{Ca}$), which determines its paleosol classification and, might represent vestiges of a contrasted rhexistasic period linked to intense surface erosion. Afterwards, the overlapping of a new basaltic lava flow may have taken place (2R horizon). This 2R horizon developed into a 2C because of the formation of $2Bt_{1\text{-}3}$, which occurred under new biostatic conditions. The $2Bt_{1\text{-}3}$ may have been formed from the accumulation of aeolian input and soil secondary soil products (i.e., illite, kaolinite, and Fe-oxides such as hematite and goethite) resulting from moderate weathering and contrasted climate conditions. This biostatic situation might have concluded with the formation of a stone line. Another biostatic period would have started with the formation of $1Bt_{1\text{-}2}$ that probably developed within a material that has the character of a slope deposit with aeolian admixtures. This period could have been characterized by moderate aeolian inputs, intense weathering, and less-contrasted climate conditions than the previous biostatic period. It may have ended with

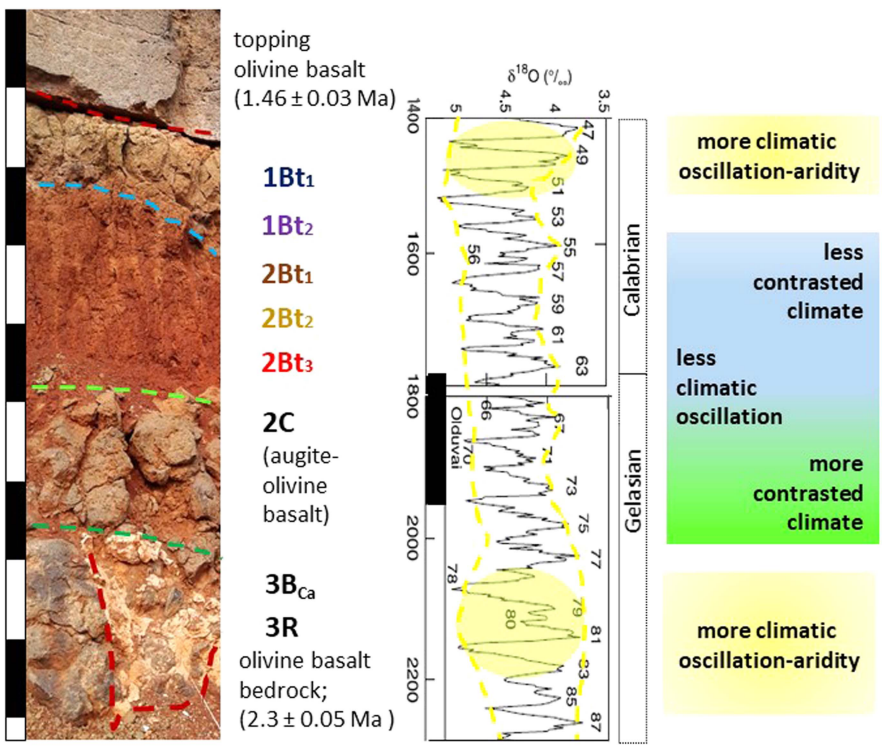

Figure 13. (color online) Hypothetical paleoclimatic evolution in Gran Canaria during the lower Pleistocene, accordingly to the global Marine Oxygen Isotope (MIS) glacial-interglacial stages, based on the variation of the climatic horizon imprints from the Ingenio paleosol. Further details in the text.

https://doi.org/10.1017/qua.2018.64 Published online by Cambridge University Press

intense erosion and the $1Bt_{1\text{-}2}$ hardening. At this point, the soil evolution could have been interrupted and the soil fossilized by a basaltic lava flow dated to 1.46 ± 0.03 Ma.

Several erosive periods may be deduced from this profile. Firstly, the residual occurrence of $3B_{Ca}$ probably resulted from the erosion of this soil in a rhexistasic period. Secondly, the stone line between the Bt horizons could be the result of an erosive interval. Thirdly, the $1Bt_{1\text{-}2}$ hardening could be due to the erosion of the vegetal cover.

Assuming a linear relationship between the quartz contents of the Ingenio paleosoils, the incorporated Saharan dust, as well as some loess-like deposits from Gran Canaria for which we expect that Saharan dust was incorporated from the early Pleistocene through the late Quaternary, we calculated the supposed Pleistocene Saharan dust input. Hence, during the lower to middle Pleistocene the dust input in the Gran Canaria profile might have been about 33–38% lower than during the middle–upper Pleistocene to late Quaternary. In addition, during the Gelasian and Calabrian periods (lower Pleistocene), we assume that the Saharan dust input on Gran Canaria has decreased, but has not disappeared entirely during the biostatic wet-warm episodes (16–30% quartz content). Finally, with respect to the early Pleistocene age, we propose that there is a direct relationship between the higher amplitude of the oxygen isotope glacial-interglacial stages and more contrasted climate conditions, as well as a higher degree of aridity, as shown in Figure 13.

ACKNOWLEDGMENTS

This work presents part of the research results arising from the projects: Materials for Advanced Power Generation (ENE2013-47826-C4-4-R) and, 3D Printed Advanced Materials for Energy Applications (ENE2016-74889-C4-2-R), both funded by Ministerio de Economía, Industria y Competitividad, Government of Spain. We want to dedicate this paper to the principal researcher of these projects, Dr. Juan Carlos Ruiz Morales who passed away too young and too recently. We thank the reviewers and editors for helpful comments and Elisabeth J. Coles for revising the linguistic style.

REFERENCES

Arbogast, A.F., Packman, S.C., 2004. Middle-Holocene mobilization of aeolian sand in western upper Michigan and the potential relationship with climate and fire. *The Holocene* 14, 464–471.

Balcells, R., Barrera, J.L., Gómez, J.A., Cueto, L.A., 1992. Mapa Geológico de España, Hoja de la Isla de Gran Canaria, Map 21-21/21-22. Instituto Tecnológico Geominero de España and Servicio de Publicaciones del Ministerio de Industria, Madrid.

Balsam, W.L., Ji, J., Chen, J., 2004. Climatic interpretation of the Luochuan and Lingtai loess section, China, based on changing iron oxide mineralogy. *Earth and Planetary Science Letters* 223, 335e348. http://dx.doi.org/10.1016/j.epsl.2004.04.023.

Barrón, V., Torrent, J., 2013. Iron, manganese and aluminum oxides and oxyhydroxides. In: Nieto, F., Livi, K.J.T., Oberti, R. (Eds.), *European Mineralogical Union Notes in Mineralogy*, *Vol. 14. Minerals at the Nanoscale,* Mineralogical Society of Great Britain and Ireland, pp. 297–336. https://doi.org/10.1180/EMU-notes.14

Bern, C.R., Yesavagea, T., Foleyb, N.K., 2017. Ion-adsorption REEs in regolith of the Liberty Hill pluton, South Carolina, USA: an effect of hydrothermal alteration. *Journal of Geochemical Exploration* 172, 29–40.

Brown, D.J., Mc Sweeney, K., Helmke, P.A., 2004. Statistical, geochemical, and morphological analyses of stone line formation in Uganda. *Geomorphology* 62, 217–237.

Campbell, M.C., Fisher, T.G., Goble, R.J., 2011. Terrestrial sensitivity to abrupt cooling recorded by aeolian activity in northwest Ohio, USA. *Quaternary Research* 75, 411–416.

Carracedo, J.C., Pérez-Torrado, F.J., Ancochea, E., Meco, J., Hernán, F., Cubas, C.R., Casillas, R., Rodríguez-Badiola, E., Ahijado, A., 2002. Cenozoic Volcanism II: The Canary Islands. In: Gibsson, W., Moreno, T. (Eds.), *The Geology of Spain*. The Geological Society, London, pp. 439–472.

Cattle, S.R., Mc Tainsh, G.H., Wagner, S., 2002. Aeolian dust contributions to soil of the Namoi Valley, northern NSW Australia. *Catena* 47, 245–264.

Chamley, H., Coudé-Gaussen, G., Debrabant, P., Rognon, P., 1987. Contribution autochtone et allochtone à la sédimentation quaternaire de l'île de Fuerteventura (Canaries): altération ou apports éoliens? *Bulletin de la Societé Géologique de France* 5, 939–952.

Chang, C., Li, F., Liu, C., Gao, J., Tong, H., Chen, M., 2016. Fractionation characteristics of rare earth elements (REEs) linked with secondary Fe, Mn, and Al minerals in soils. *Acta Geochimica* 35, 329.

Cita, M.B., Pillans, B., 2010. Global stages, regional stages or no stages in the Plio/Pleistocene? *Quaternary International* 219, 6–15.

Cornell, R.M., Schwertmann, U., 2003. *The Iron Oxides Structure, Properties, Reactions, Occurrences and Uses*. 2nd Edition, Wiley-VCH, Weinheim.

Criado, C., Dorta, P., 2003. An unusual ''blood rain'' over the the Canary Islands (Spain):the storm of January 1999. *Journal of Arid Environments* 55, 765–783.

Dorta, P., 1999. Las invasiones de aire sahariano en Canarias [The advections of Saharan air in the Canary Islands]. Consejería de Agricultura, Pesca y Alimentación del Gobierno de Canarias y Caja Rural de Tenerife, Santa Cruz de Tenerife.

Dupont, L., Leroy, S., 1995. Steps toward drier climatic conditions in Northwestern Africa during the Upper Pliocene. In: Vrba, E., Denton, G., Burckle, L., Partridge, T. (Eds.), *Paleoclimate and Evolution*. Yale University Press, New Haven, pp. 289–298.

Ehrmann, W., Schmiedl, G., Beuscher, S., Krüger, S., 2017. Intensity of African Humid Periods Estimated from Saharan Dust Fluxes. *PLoS ONE* 12(1), e0170989. http://dx.doi.org/10.1371/journal.pone.0170989.

Engelstaedter, S., Tegen, I., Washington, R., 2006. North African dust emissions and transport. *Earth-Science Reviews* 79, 73–100.

Erhart, H., 1955. "Biostasie" et "rhexistasie": esquisse d'une théorie sur le rôle de la pédogenèse en tant que phénomène géologique. *Comptes Rendus Académie des Sciences* 241, 1218–1220.

Faust, D., Yurena, Y., Willkommen, T., Roettig, C., Richter, D., Richter, D., v. Suchodoletz, H., Zöller, L., 2015. A contribution to the understanding of late Pleistocene dune sand-paleosol-sequences in Fuerteventura (Canary Islands). *Geomorphology* 246, 290–304.

Fedoroff, N., Courty, M.A., Guo, Z.T., 2010. Palaeosols and relict soils. In: Stoops, G., Marcelino, V., Mees, F. (Eds), *Interpretation*

of Micromorphological Features of Soils and Regoliths. Elsevier, Amsterdam, pp. 623–662.

Forman, S.L., Oglesby, R., Webb, R.S., 2001. Temporal and spatial patterns of Holocene dune activity on the Great Plains of North America: megadroughts and climate links. *Global and Planetary Change* 29, 1–29.

Gibbard, P.L., Head, M.J., 2009. IUGS ratification of the Quaternary System/Period and the Pleistocene Series/Epoch with a base at 2.58 Ma. *Quaternaire* 20, 411–412.

Goudie, A., 2013. *Encyclopedia of Geomorphology*. Taylor and Francis, https://books.google.es/books?id=JJHyXx42OQEC.

Goudie, A.S., Middleton, N.J., 2001. Saharan dust storms: nature and consequences. *Earth-Science Reviews* 56, 179–204.

Guillou, H., Perez Torrado, F.J., Hansen Machin, A.R, Carracedo, J.C., Gimeno, D., 2004. The Plio–Quaternary volcanic evolution of Gran Canaria based on new K–Ar ages and magnetostratigraphy. *Journal of Volcanology and Geothermal Research* 135, 221–246.

Hallam, A., Grose, J.A., Ruffell, A.H., 1991. Palaeoclimatic significance of changes in clay mineralogy across the Jurassic-Cretaceous boundary in England and France. *Palaeogeography, Palaeoclimatology, Palaeoecology* 81, 173–187.

Hamann, Y., Ehrmann, W., Schmiedl, G., Krüger, S., Stuut, J.-B., Kuhnt, T., 2008. Sedimentation processes in the Eastern Mediterranean Sea during the Late Glacial and Holocene revealed by end-member modelling of the terrigenous fraction in marine sediments. *Marine Geology* 248, 97–114.

Hansen, E.C., Fisher, T.G., Arbogast, A.F., Bateman, M.D., 2010. Geomorphic history of low-perched, transgressive dune complexes along the southeastern shore of Lake Michigan. *Aeolian Research* 1, 111–127.

Henderiks, J., Freudenthal, T., Meggers, H., Navec, S., Abrantesc, F., Bollmanna, J., Thierstein, H.R., 2002. Glacial-interglacial variability of particle accumulation in the Canary Basin: a time-slice approach. *Deep-Sea Research Part II: Topical Studies in Oceanography* 49, 3675–3705.

Hooghiemstra, H., Lézine, A.-M., Leroy, S.A.G., Dupont, L., Marret, F., 2006. Late Quaternary palynology in marine sediments: a synthesis of the understanding of pollen distribution patterns in the NW African setting. *Quaternary International* 148, 29–44.

Hong, H., Gu, Y., Li, R., Zhang, K., Li, Z., 2010. Clay mineralogy and geochemistry and their palaeoclimatic interpretation of the Pleistocene deposits in the Xuancheng section, southern China. *Journal of Quaternary Science* 25, 662–674.

Hong, H., Gu, Y., Yin, K., Wang, C., Li, Z., 2013. Clay record of climate change since themid-Pleistocene in Jiujiang, south China. *Boreas* 42, 173–183.

Ji, J., Balsam, W., Chen, J., 2001. Mineralogic and climatic interpretations of the Luochuan loess section (China) based on diffuse reflectance spectrophotometry. *Quaternary Research* 56, 23–30.

Johnson, D.L., Domier, J.E.J., Johnson, D.N., 2005. Animating the biodynamics of soil thickness using process vector analysis: a dynamic denudation approach to soil formation. *Geomorphology* 67, 23–46.

Kettler, T.A., Doran, J.W., Gilbert, T.L., 2001. *Simplified Method for Soil Particle-Size Determination to Accompany Soil-Quality Analyses*. Publications from USDA-ARS / UNL Faculty, 305. http://digitalcommons.unl.edu/usdaarsfacpub/305.

Kukla, G., Han, Z., 1989. Loess stratigraphy in Central China. *Palaeogeography, Palaeoclimate, Palaeoecology* 72, 200–225.

Küster, Y., Hetzel, R., Krbetschek, M., Tao, M.X., 2006. Holocene loess sedimentation along the Qilian Shan (China): significance for understanding the processes and timing of loess deposition. *Quaternary Science Reviews* 25, 114–125.

Lafon, S., Rajot, J.L., Alfaro, S.C., Gaudichet, A., 2004. Quantification of iron oxides in desert aerosol. *Atmospheric Environment* 38, 1211–1218.

Lázaro, F.J., Gutiérrez, L., Barrón, V., Gelado, M.D., 2008. The speciation of iron in desert dust collected in Gran Canaria (Canary Islands): combined chemical, magnetic and optical analysis. *Atmospheric Environment* 42, 8987–8996.

Lehmkuhl, F., Schulte, P., Zhao, H., Hülle, D., Protze, J., Stauch, G., 2014. Timing and spatial distribution of loess and loess-like sediments in the mountain areas of the northeastern Tibetan Plateau. *Catena* 117, 23–33.

Leroy, S.A.G., 2007. Progress in palynology of the Gelasian–Calabrian Stagesin Europe: ten messages. *Revue de Micropaléontologie* 50, 293–308.

Leroy, S.A.G., Dupont, L.M., 1997. Marine palynology of the ODP 658 (N-W Africa) and its contribution to the stratigraphy of Late Pliocene. *Geobios* 30, 351–359.

Lisiecki, L.E., Raymo, M.E., 2005. A Pliocene-Pleistocene stack of 57 globally distributed benthic δ18O records. *Paleoceanography* 20, PA1003. http://dx.doi.org/10.1029/2004PA001071.

Liu, X.-J., Xiao, G., E, C., Li, X., Lai, Z., Yu, L., Wang, Z., 2017. Accumulation and erosion of aeolian sediments in the north-eastern Qinghai-Tibetan Plateau and implications for provenance to the Chinese Loess Plateau. *Journal of Asian Earth Sciences* 135, 166–174.

Long, X., Ji, J., Balsam, W., 2011. Rainfall-dependent transformations of iron oxides in a tropical saprolite transect of Hainan Island, South China: spectral and magnetic measurements. *Journal of Geophysical Research Earth Surface* 116, 1–15.

Long, X., Ji, J., Barrón, V., Torrent, J., 2016. Climatic thresholds for pedogenic iron oxides under aerobic conditions: processes and their significance in paleoclimate reconstruction. *Quaternary Science Reviews* 150, 264–277.

Loope, W.L., Arbogast, A.F., 2000. Dominance of an ~150-year cycle of sand-supply change in Late Holocene dune-building along the eastern shore of Lake Michigan. *Quaternary Research* 54, 414–422.

Lu, H.Y., Zhao, C.F., Mason, J., Yi, S.W., Zhao, H., Zhou, Y.L., Ji, J.F., Swinehart, J., Wang, C.M., 2010. Holocene climatic changes revealed by aeolian deposits from the Qinghai Lake area (north eastern Qinghai-Tibetan Plateau) and possible forcing mechanisms. *The Holocene* 21, 297–304.

Mangas, J., Pérez-Torrado, J.F., Gimeno, D., Hansen, A., Paterne, M., Guillou, H., 2002. Caracterización de los materiales volcánicos asociados a las erupciones holocenas de la Caldera de Pinos de Galdar y edificios volcánicos adyacentes (Gran Canaria). *Geogaceta* 32, 49–52.

Mason, J.A., Joeckel, R.M., Bettis, E.A. III, 2007. Middle to Late Pleistocene loess record in eastern Nebraska, USA, and implications for the unique nature of Oxygen Isotope Stage 2. *Quaternary Science Reviews* 26, 773–792.

Mbagwu, J.S.C., 2008. *From Paradox to Reality: Unfolding the Discipline of Soil Physics in Soil Science*. University of Nigeria, Nsukka.

McLennan, S.M., Hemming, S., McDaniel, D.K., Hanson, G.N., 1993. Geochemical approaches to sedimentation, provenance, and tectonics. In: Johnsson, M.J., Basu, A. (Eds.), *Processes*

Controlling the Composition of Clastic Sediments. Geological Society of America, Special Papers 284, 21–40.

Meco, J., Guillou, H., Carracedo, J.C., Lomoschitz, A., Ramos, A.-J.G., Rodríguez-Yánez, J.J., 2002. The maximum warmings of the Pleistocene world climate recorded in the Canary Islands. *Palaeogeography, Palaeoclimate, Palaeoecology* 185, 197–210.

Meco, J., Koppers, A.A.P., Miggins, D.P., Lomoschitz, A., Betancort, J.F., 2015. The Canary record of the evolution of the North Atlantic Pliocene: new 40Ar/39Ar ages and some notable palaeontological evidence. *Palaeogeograpdy, Palaeoclimate, Palaeoecology* 435, 53–69.

Mehra, O.P., Jackson, M.L., 1958. Iron oxide removal from soils and clays by a dithionite-citrate system buffered with sodium bicarbonate. *Clays and Clay Minerals* 7, 317–327.

Menéndez, I., Cabrera, L., Sánchez-Pérez, I., Mangas, J., Alonso, I., 2009a. Characterisation of two fluvio-lacustrine loessoid deposits on the island of Gran Canaria, The Canary Islands. *Quaternary International* 196, 36–43.

Menéndez, I., Derbyshire, E., Carrillo, T., Caballero, E., Engelbrecht, J.P., Romero, L.E., Mayer, P.L., Rodríguez de Castro, F., Mangas, J., 2017. Saharan dust and the impact on adult and elderly allergic patients: the effect of threshold values in the northern sector of Gran Canaria, Spain. *International Journal of Environmental Health Research* 27, 144–160.

Menéndez, I., Derbyshire, E., Engelbrecht, J., von Suchodoletz, H., Zöller, L., Dorta, P., Carillo, T., Rodríguez de Castro, F., 2009b. Saharan dust and the aerosols on the Canary Islands: past and present. In: Cheng, M., Liu, W. (Eds.), *Airborne Particulates*. Novapublishers, Hauppauge, NY, pp. 39–80.

Menéndez, I., Díaz-Hernandez, J.L., Mangas, J., Alonso, I., Sánchez-Soto, P.J., 2007. Airborne dust accumulation and soil development in the north-east sector of Gran Canaria (Canary Island, Spain). *Journal of Arid Environment* 71, 57–81.

Morales, J., Rodríguez, A., Alberto, V., Machado, C., Criado, C., 2009. The impact of human activities on the natural environment of the Canary Islands (Spain) during the pre-Hispanic stage (3rd–2nd Century BC to 15th Century AD): an overview. *Environmental Archaeology* 14, 27–36.

Morrás, H., Moretti, L., Píccolo, G., Zech, W., 2006. Stone lines and weathering profiles of ferralitic soils in Northeastern Argentina. In *Proceedings of the workshop for Alumni of the M.Sc. programmes in Soil Science, Eremology and Physical Land Resource*. Gent University, Gent, Belgium, pp. 269–279.

Muhs, D.R., Budahn, J. R., Prospero, J. M., Carey, S. N., 2007. Geochemical evidence for African dust inputs to soils of western Atlantic islands: Barbados, the Bahamas, and Florida. *Journal of Geophysical Research* 112, F02009. http://dx.doi.org/10.1029/2005JF000445.

Muhs, D.R., Bush, C.A., Stewart, K.C., Rowland, T.R., 1990. Geochemical evidence of Saharan dust parent material for soils developed on Quaternary limestones of Caribbean and western Atlantic islands. *Quaternary Research* 33, 157–177.

Neff, J.C., Ballantyne, A.P., Farmer, G.L., Mahowald, N., Conroy, J.L., Landry, C.C., Overpeck, J.T., Painter, T.H., Lawrence, C.R., Reynolds, R.L., 2008. Increasing eolian dust deposition in the western United States linked to human activity. *Nature Geosciences* 1. http://dx.doi.org/10.1038/ngeo 2008.

Nesbitt, H.W., Young, G.M., 1989. Formation and diagenesis of weathering profiles. *Journal of Geology* 97, 129–147.

Nettleton, W.D., Olson, C.G., Wysocki, D.A., 2000. Palaeosol classification: problems and solutions. *Catena* 41, 61–92.

Offer, Z.Y., Zaady, E., Shachak, M., 1998. Aeolian particle input to the soil surface at the northern limit of the Negev desert. *Arid Soil Research and Rehabilitation* 12, 55–62.

Olson, C.G., Nettleton, W.D., 1998. Palaeosols and the effects of alteration. *Quaternary International* 51/52, 185–194.

Pokras, E.M., 1989. Pliocene history of South Saharan/Sahelian aridity: record of freshwater diatoms (Genus Melosira) and opal phytoliths, ODP sites 662 and 664. In: Leinen, M., Sarnthein, M. (Eds.), *Palaeoclimatology and Palaeometeorology: Modern and Past Patterns of Global Atmospheric Trans-port*. Kluwer Academic Publishing, Dordrecht, pp. 795–804.

Price, J.R., Velbel, M.A., 2003. Chemical weathering indices applied to weathering profiles developed on heterogeneous felsic metamorphic parent rocks. *Chemical Geology* 202, 397–416.

Prospero, J.M., 1996. Dust transport over the North Atlantic Ocean and Mediterranean: an overview. In: Guerzoni S., Chester R. (Eds.), *The Impact of Desert Dust Across the Mediterranean*. Kluwer Academic Publishing, Dordrecht, pp. 133–151.

Prospero, J.M., Lamb, P.J., 2003. African Droughts and Dust Transport to the Caribbean: Climate Change Implications. *Science* 302, 1024.

Qiang, M.R., Chen, F.H., Song, L., Liu, X.X., Li, M.Z., Wang, Q., 2013. Late Quaternary aeolian activity in Gonghe Basin, northeastern Qinghai-Tibetan Plateau. *Quaternary Research* 79, 403–412.

Qiang, M.R., Jin, Y.X., Liu, X.X., Song, L., Li, H., Li, F.S., Chen, F. H., 2016. Late Pleistocene and Holocene aeolian sedimentation in Gonghe Basin, northeastern Qinghai-Tibetan Plateau: variability, processes, and climatic implications. *Quaternary Science Reviews* 132, 57–73.

Rodríguez, S., Alastuey, A., Alonso-Pérez, S., Querol, X., Cuevas, E., Abreu-Afonso, J., Viana, M., Pérez, N., Pandolfi, M., de la Rosa, J., 2011. Transport of desert dust mixed with North African industrial pollutants in the subtropical Saharan air layer. *Atmospheric Chemistry Physics* 11, 6663–6685.

Roettig, C.-B., Varga, G., Sauer, D., Kolb, T., Wolf, D., Makowsky, V., Recio Espejo, J.M., Zöller, L., Faust, D., 2018. Characteristics, nature and formation of palaeosurfaces within dunes on Fuerteventura. *Quaternary Research*, doi:10.1017/qua.2018.52.

Runge, J., 2001. On the age of stone-lines and hillwash sediments in the eastern Congo basin – palaeoenvironmental implications. *Palaeoecology of Africa and the Surrounding Islands* 27, 19–36.

Sadeghi, M., Petrosino, P., Ladenberger, A., Albanese, S., Andersson, M., Morris, G., Lima, A., De Vivo, B., the GEMAS Project Team. 2013. Ce, La and Y concentrations in agricultural and grazing-land soils of Europe. *Journal of Geochemical Exploration* 133, 202–213.

Santana, I.V., Wall, F., Botelho, N.F., 2015. Occurrence and behavior of monazite-(Ce) and xenotime-(Y) in detrital and saprolitic environments related to the Serra Dourada granite, Goiás/Tocantins State, Brazil: Potential for REE deposits. *Journal of Geochemical Exploration* 155, 1–13.

Scheinost, A.C., Chavernas, A., Barrón, V., Torrent, J., 1998. Use and limitations of second-derivative diffuse reflectance spectroscopy in the visible to near-infrared range to identify and quantify Fe oxides in soils. *Clays and Clay Minerals* 46, 528–537.

Scheuvens, D., Schütz, L., Kandler, K., Ebert, M., Weinbruch, S., 2013. Bulk composition of northern African dust and its source sediments — a compilation. *Earth-Science Reviews* 116, 170–194.

Schmincke, H., Sumita, M., 2010. Geological evolution of the Canary Islands: a young volcanic archipelago adjacent to the old

African Continent. Ed. Görres Druckerei und Verlag GmbH, Koblenz, Germany.

Schwertmann, U., 1964. Differenzierung der Eisenoxide des Bodens durch Extraktion mit sauerAmmoniumoxalat-Lösung. *Zeitschrift fur Pflanzenernahrung und Bodenkunde* 105, 194–202.

Shackleton, N.J., Crowhurst, S., Hagelberg, T., Pisias, N.G., Schneider, D.A., 1995. A new Late Neogene time scale: applications to leg 138 sites. In: Pisias, N.G., Mayer, L.A., Janecek, T.R., Palmer-Julson, A., van Andel, T.H. (Eds.), *Proceedings ODP, Scientific Results 138*. Ocean Drilling Program, College Station, TX, pp. 73–101.

Sunnu, A., Afeti, G., Resch, F., 2008. A long-term experimental study of the Saharan dust presence in West Africa. *Atmospheric Research* 87, 13–26.

Timmons, E.A., Fisher, T.G., Hansen, E.C., Eiasman, E., Daly, T., Kashgarian, M., 2007. Elucidating eolian dune history from lacustrine sand records in the Lake Michigan coastal zone, USA. *The Holocene* 17, 789–801.

Torrent, J., Barrón, V., 2002. Diffuse reflectance spectroscopy of iron oxides. In: Hubbard, A.T. (Ed.), *Encyclopedia of Surface and Colloid Science* Vol 1. Marcel Dekker, New York, pp. 1438–1446.

Torrent, J., Liu, Q., Bloemendl, J., Barron, V., 2007. Magnetic enhancement and iron oxides in the upper Luochuan loess-palaeosol sequence, Chinese Loess Plateau. *Soil Science Society of America Journal* 71, 1570–1578.

Tyler, G., 2004. Rare earth elements in soil and plant systems - a review. *Plant Soil* 267, 191–206.

Újvári, G., Kok, J.F., Varga, G., Kovács, J., 2016. The physics of wind-blown loess: Implications for grain size proxy interpretations in Quaternary paleoclimate studies. *Earth-Science Reviews* 15, 247–278.

von Suchodoletz, H., Faust, D., Zöller, L., 2009a. Geomorphological investigations of sediment traps on Lanzarote (Canary Islands) as a key for the interpretation of a palaeoclimate archive off NW Africa. *Quaternary International* 196, 44–56.

von Suchodoletz, H., Fuchs, M., Zöller, L., 2008. Dating Saharan dust deposits at Lanzarote (Canary Islands) by luminescence dating techniques and their implication for paleoclimate reconstruction of NW Africa. *Geochemistry, Geophysics, and Geosystems* 9, 1–19.

von Suchodoletz, H., Glaser, B., Thrippleton, T., Broder, T., Zang, U., Eigenmann, R., Kopp, B., Reichert, M., Zöller, L., 2013. The influence of Saharan dust deposits on La Palma soil properties (Canary Islands, Spain). *Catena* 103, 44–52.

von Suchodoletz, H., Kühn, P., Hambach, U., Dietze, M., Zöller, L., Faust, D., 2009b. Loess-like and palaeosol sediments from Lanzarote (Canary Islands/Spain) -indicators of palaeoenvironmental change during the Late Quaternary. *Palaeogeography, Palaeoclimate, Palaeoecology* 278, 71–87.

Wilkinson, M.T., Richards, P.J., Humphreys, G.S., 2009. Breaking ground: pedological, geological, and ecological implications of soil bioturbation. *Earth Science Reviews* 97, 254–269.

Wolfe, S.A., Hugenholtz, C.H., 2009. Barchan dunes stabilized under recent climate warming on the northern Great Plains. *Geology* 37, 1039–1042.

Wolfe, S.A., Huntley, D.A., Ollerhead, J., 2004. Relict Late Wisconsinan dune fields of the northern Great Plains. *Canada Geographie physique et Quaternaire*. 58, 323–326.

Yang, S., Ding, F., Ding, Z., 2006. Pleistocene chemical weathering history of Asian arid and semi-arid regions recorded in loess deposits of China and Tajikistan. *Geochimica et Cosmochimica Acta* 70, 1695–1709.

Yu, L.P., Lai, Z.P., 2012. OSL chronology and palaeoclimatic implications of Aeolian sediments in the eastern Qaidam Basin of the northeastern Qinghai-Tibetan Plateau. *Palaeogeography, Palaeoclimate, Palaeoecology* 337–338, 120–129.

Zeng, L., Lua, H., Yi, S., Stevens, T., Xu, Z., Zhuo, H., Yu, K., Zhang, H., 2017. Long-term Pleistocene aridification and possible linkage to high-latitude forcing: new evidence from grain size and magnetic susceptibility proxies from loess-palaeosol record in northeastern China. *Catena* 154, 21–32.

Zhang, J.R., Nottebaum, V., Tsukamoto, S., Lehmkuhl, F., Frechen, M., 2015. Late Pleistocene and Holocene loess sedimentation in central and western Qilian Shan (China) revealed by OSL dating. *Quaternary International* 372, 120–129.

Zhang, W., Yu, L., Lu, M., Zheng, X., Ji, J., Zhou, L., Wang, X., 2009. East Asian summer monsoon intensity inferred from iron oxide mineralogy in the Xiashu Loess in southern China. *Quaternary Science Reviews* 28, 345–353.

Zhao, L., Honga, H., Fanga, Q., Yina, K., Wang, C, Li, Z, Torrent, J, Cheng, F, Algeoa, T.J., 2017. Monsoonal climate evolution in southern China since 1.2 Ma: New constraints from Fe-oxide records in red earth sediments from the Shengli section, Chengdu Basin. *Paleogeography, Palaeoclimate, Palaeoecology* 473, 1–15.

https://doi.org/10.1017/qua.2018.64 Published online by Cambridge University Press